Spectral Signature of Relaxation Oscillations in Semiconductor Lasers

M. P. van Exter, W. A. Hamel, J. P. Woerdman, and B. R. P. Zeijlmans

Abstract—**A new and relatively simple expression is given for the optical spectrum of a single-mode semiconductor laser which, due to the presence of relaxation oscillations, consists of a strong central line with a broad weak sideband at each side. The coupling between phase and amplitude fluctuations is included in this derivation and is shown to result in an asymmetry between the relaxation oscillation sidebands. This asymmetry can be used to determine the linewidth enhancement factor α. Using optical heterodyne detection we have accurately measured the spectrum of a Fabry–Perot-type AlGaAs laser as a function of output power. Information on the dynamics of the relaxation oscillations was thus obtained. The power dependence of the frequency and damping of the relaxation oscillations allowed us to separately determine the spontaneous lifetime and the dependence of the gain on both carrier density (differential gain) and intensity (gain saturation).**

I. Introduction

VAHALA, Harder, and Yariv (VHY) [1] were the first to link the broad weak sidebands observed around the central frequency of a semiconductor laser with the presence of relaxation oscillations, which result from the interplay between the intracavity optical intensity and the population inversion [1]–[8]. Up to now a simple expression for the optical spectrum in the presence of relaxation oscillations has been lacking. It is common practice to neglect the amplitude fluctuations and include only the phase fluctuations, as they give the strongest contribution to the spectrum [6]. In our treatment both fluctuations are taken into account. Especially the coupling between phase and amplitude is seen to influence the spectrum, it leads to an asymmetry, as already noticed by VHY.

Starting from the linearized laser equations [9] we evaluate in this paper the time auto-correlation and cross-correlation functions of the phase and amplitude fluctuations of the intracavity optical field. These are Fourier related to the optical spectrum of the laser light for which we give an approximate expression. From this expression we draw several conclusions about, e.g., the relative intensity of the relaxation oscillation sidebands and their non-Lorentzian component.

Manuscript received April 5, 1991; revised December 20, 1991. This work was supported by the Nederlandse Organisatie voor Wetenschappelijk Onderzoek (NWO) and is part of the Research Program of the Stichting voor Fundamenteel Onderzoek der Materie (FOM).

The authors are with Huygens Laboratory, University of Leiden, 2300 RA Leiden, The Netherlands.

IEEE Log Number 9107791.

The laser spectrum with relaxation oscillation sidebands shown by VHY was measured with a Fabry–Perot etalon and had therefore a limited spectral resolution, which made precise quantitative analysis of the data difficult. Heterodyne detection, based on coherent mixing, is a superior technique for spectral measurements [10]. We have used heterodyne detection to measure the optical field spectrum of a Hitachi HLP1400 laser as a function of output power. The excellent fit between theory and experiment has allowed us to study the power dependence of both the relaxation oscillation frequency and damping rate. Hereby we could separate the damping rate in the lifetime-related part and the contributions due to the differential gain and gain saturation. Also, we introduce a new technique to determine the linewidth enhancement factor α, based on the asymmetry between the low- and high-frequency sideband. Here again we profit from the excellent fit between theory and experiment.

II. Basic Equations

In this section the basic variables and equations needed to describe the laser operation are introduced. We consider a single-mode laser and introduce the slowly varying amplitude $E(t)$ of the intracavity optical field Re $[E(t)e^{i\omega_l t}]$, where ω_l is the central frequency. According to the Wiener–Khintchine theorem the (shifted) optical spectrum is Fourier-related to the normalized time-autocorrelation function of the optical field [7]

$$G_E(t) = \langle E(t' + t)E^*(t')\rangle / \langle |E(t')|^2 \rangle \tag{1}$$

where $\langle\ \rangle$ denotes time averaging over t'. It is our aim to evaluate this autocorrelation function from the standard laser equations [7]

$$\frac{d}{dt}E(t) = \frac{1}{2}(G_{\text{eff}} - \Gamma_c)E(t) + F_{\text{sp}}(t) \tag{2a}$$

$$\frac{d}{dt}N(t) = \frac{I}{eV} - \frac{N(t)}{T_{\text{sp}}} - G_r \mathcal{S}(t). \tag{2b}$$

Here Γ_c is the cavity loss rate, $G_{\text{eff}} = \Gamma G$ is the effective gain rate, Γ the confinement factor (being the fraction of the optical intensity inside the active layer), $\frac{1}{2}G = \frac{1}{2}\{G_r + iG_i\}$ the (complex) bulk amplitude gain rate, $F_{\text{sp}}(t)$ the spontaneous-emission noise, $N(t)$ the carrier density, I is the injected current, e is the electron charge, V is the active volume, T_{sp} is the carrier-recombination time, and $\mathcal{S}$

the photon density, i.e., the average number of photons in the laser mode divided by the optical mode volume (V/Γ). The photon density is proportional to the square of the optical field inside the cavity.

The standard laser equations are linearized by expanding the optical field, the population inversion and the complex gain G_{eff} around their stationary values,

$$E(t) = E_0 e^{-u(t)} e^{i\phi(t)} \tag{3a}$$

$$N(t) = N_0 + n(t) \tag{3b}$$

$$G_{\text{eff}} = \Gamma_c + \left.\frac{\partial G_{\text{eff}}}{\partial N}\right|_{N_0} n(t) + \left.\frac{\partial G_{\text{eff}}}{\partial S}\right|_{N_0} \Delta \mathcal{S}(t). \tag{3c}$$

Notice that the dependence of the gain on both the carrier density and the intensity is taken into account. In the literature the intensity dependence of the optical gain, which we denote here by gain saturation, is also referred to as nonlinear gain. Gain saturation is generally ascribed to spatial and spectral redistribution of the carriers (hole burning), dynamic carrier heating, population pulsations or combinations thereof [12]–[15]. Gain saturation being small, it is often removed from the laser equations [9], [17]. However, our experiments show gain saturation to be of crucial importance in describing the dynamics of the relaxation oscillations far above threshold. At large output powers it even dominates the damping of the relaxation oscillations.

The intensity dependence of the gain is usually quantified by the gain-saturation coefficient κ_S as

$$G(N, \mathcal{S}) = \frac{G(N, 0)}{1 + \kappa_S \mathcal{S}} \tag{4}$$

where $G(N, 0)$ is the small-signal gain (for $\mathcal{S} \approx 0$). If one considers spectral hole burning as the prime source of gain saturation (4) would have a different form [16]

$$G(N, \mathcal{S}) = \frac{G(N, 0)}{\sqrt{1 + 2\kappa_S \mathcal{S}}}. \tag{5}$$

However, as discussed in section V, we find that, under our experimental conditions (output power $P_{\text{out}} \leq 20$ mW), the product $\kappa_S \mathcal{S}$ is very small ($\kappa_S \mathcal{S} \leq 0.01$) so that the difference between (4) and (5) is negligible. As a consequence, (3c) can be rewritten in the following form

$$G_{\text{eff}} = \Gamma_c + \xi(1 + i\alpha)n(t) + 2\Gamma_c \kappa_S \mathcal{S}_0 u(t) \tag{6}$$

where ξ is the effective differential gain, α is the linewidth-enhancement factor [11], $\Delta \mathcal{S}(t) = -2u(t)\mathcal{S}_0$, and $\mathcal{S}_0$ is the average photon density. Note that for InGaAsP lasers κ_S is generally much larger than for AlGaAs lasers, so that a first-order expansion is in practice not always valid.

The linearized laser equations are

$$\frac{d}{dt} u(t) = -\frac{1}{2} \xi n(t) - \Gamma_c \kappa_S \mathcal{S}_0 u(t) + f_{1,\text{sp}}(t) \tag{7a}$$

$$\frac{d}{dt} \phi(t) = \frac{1}{2} \alpha \xi n(t) + f_{2,\text{sp}}(t) \tag{7b}$$

$$\frac{d}{dt} n(t) = -\left(\frac{1}{\tau_{\text{sp}}} + \xi \mathcal{S}_0/\Gamma\right) n(t) + \frac{2\omega_0^2}{\xi} u(t) \tag{7c}$$

where τ_{sp} is the spontaneous lifetime, defined as $\tau_{\text{sp}}^{-1} = \partial(N/T_{\text{sp}})/\partial N$ [18] and ω_0 is defined below. The so-called Langevin noise sources $f_{1,\text{sp}}(t)$ and $f_{2,\text{sp}}(t)$ are proportional to $F_{\text{sp}}(t)$ and denote the contribution of spontaneous emission to the optical field [4]. They are Gaussian-distributed random variables assumed to have a white frequency spectrum and completely characterized by the correlation

$$\langle f_{i,\text{sp}}(t' + t) f_{j,\text{sp}}^*(t') \rangle = D\, \delta_{ij}\, \delta(t). \tag{8}$$

D is the phase diffusion coefficient in [rad^2 s^{-1}] given by

$$D = n_{\text{sp}} \frac{\Gamma_c}{2\mathcal{S}_0(V/\Gamma)} K \tag{9}$$

where $n_{\text{sp}} = N_2/(N_2 - N_1)$ is the so-called excess spontaneous emission factor [4], [7], $\mathcal{S}_0(V/\Gamma)$ is recognized as the average number of photons in the laser mode and K is the excess-noise factor [19].

The linearized laser equations (7a)–(7c) can be solved by Fourier analysis [4]. Transformed into the frequency domain this set of equations shows a resonance at $\omega = 0$, which corresponds to phase diffusion, and resonances at $\omega = \pm\omega_r + i\gamma_r$, where [7], [17]

$$\omega_r = \sqrt{\omega_0^2 - \gamma_r^2 + \Gamma_c \kappa_S \mathcal{S}_0 \left(\frac{1}{\tau_{\text{sp}}} + \xi \mathcal{S}_0/\Gamma\right)} \tag{10a}$$

$$\omega_0 = \sqrt{\xi \Gamma_c \mathcal{S}_0/\Gamma} \tag{10b}$$

$$\gamma_r = \frac{1}{2}\left(\frac{1}{\tau_{\text{sp}}} + \xi \mathcal{S}_0/\Gamma + \Gamma_c \kappa_S \mathcal{S}_0\right) \tag{10c}$$

$$\gamma_n = \frac{1}{2}\left(\frac{1}{\tau_{\text{sp}}} + \xi \mathcal{S}_0/\Gamma\right). \tag{10d}$$

The resonances at $\omega = \pm\omega_r + i\gamma_r$ correspond to relaxation oscillations, which physically result from the coupling between the intensity and the population inversion, via stimulated emission. Equation (10c) shows the damping rate γ_r of the relaxation oscillations to arise from three sources, namely the finite spontaneous lifetime and the influence of the differential gain and gain saturation. The symbol γ_n has been introduced to denote the damping rate arising from the first two processes only. Close to threshold only the lifetime-related damping is important. Far above threshold both power-dependent contributions become significant. The difference between ω_r and ω_0 is usually negligible (e.g., $<2\%$ for the measurements plotted in Figs. 6 and 7 below).

III. Time-Correlation Functions and Spectrum

The linearized laser equations can be solved by Fourier analysis as was demonstrated by Henry [4] for the phase–

phase correlation function. Below, expressions are given for all three relevant correlation functions [17]. In many practical situations the relaxation oscillations are well resolved ($\gamma_r << \omega_0$). We simplify the algebra by discarding terms smaller by a factor $(\gamma_r/\omega_0)^2$ than the leading term. Via Fourier analysis one finds (for $t > 0$)

$$\langle[\phi(t'+t)-\phi(t')]^2\rangle = D(\alpha^2+1)t + \left\{\frac{D\alpha^2}{2\gamma_r}\right\}\{1-e^{-\gamma_r t}\cos(\omega_r t)\} - \left\{\frac{3D\alpha^2}{2\omega_r}\right\}e^{-\gamma_r t}\sin(\omega_r t) \quad (11a)$$

$$\langle[u(t'+t)+u(t')][\phi(t'+t)-\phi(t')]\rangle = \left\{\frac{2D\alpha\gamma_n}{\omega_r^2}\right\}\{1-e^{-\gamma_r t}\cos(\omega_r t)\} + \left\{\frac{D\alpha\gamma_n}{\omega_r\gamma_r}\right\}e^{-\gamma_r t}\sin(\omega_r t) \quad (11b)$$

$$\langle[u(t'+t)+u(t')]^2\rangle = \left\{\frac{D}{2\gamma_r}\right\}\{1+e^{-\gamma_r t}\cos(\omega_r t)\} - \left\{\frac{D}{2\omega_r}\right\}e^{-\gamma_r t}\sin(\omega_r t) \quad (11c)$$

where $\langle\ \rangle$ denotes time-averaging over t'. Notice that the correlation functions contain either the *phase difference* $[\phi(t+t')-\phi(t')]$ or the *amplitude sum* $[u(t+t')+u(t')]$.

The above functions are sufficient to evaluate the correlation function of the optical field $G_E(t)$ and to obtain the optical spectrum by Fourier transformation. This procedure is made easier by the fact that the fluctuating variables $d\phi(t)/dt$ and $u(t)$ result from a normally distributed ergodic stationary process [6]. In [17] it is shown how, for a bivariate Gaussian probability function, the brackets $\langle\ \rangle$ can be moved into the exponent

$$\begin{aligned} G_E(t) &= \langle E(t'+t)E^*(t')\rangle/\langle E^2(t')\rangle \\ &= \langle\exp\{-[u(t'+t)+u(t')]\} \cdot \exp\{i[\phi(t'+t)-\phi(t')]\}\rangle/\langle e^{-2u(t')}\rangle \\ &= \exp\left(-\tfrac{1}{2}\{\langle[\phi(t'+t)-\phi(t')]^2\rangle - \langle[u(t'+t)+u(t')]^2\rangle + 4\langle u(t')]^2\rangle\}\right) \\ &\quad \cdot \exp\{-i\langle[u(t'+t)+u(t')] \cdot [\phi(t'+t)-\phi(t')]\rangle\}. \end{aligned} \quad (12)$$

The real part of $G_E(t)$ is symmetric in time and corresponds with the symmetric part of the spectrum, i.e., the part that is even in $(\omega-\omega_l)$. The imaginary part of $G_E(t)$, reflecting the coupling between the amplitude and phase fluctuations, is antisymmetric in time and corresponds to the antisymmetric part of the spectrum, i.e., the part that is odd in $(\omega-\omega_l)$.

In many practical cases the central laser line is narrow compared to the relaxation oscillation sidebands, i.e., $D(\alpha^2+1) << \gamma_r$, and the above expression for $G_E(t)$ can be expanded in $D(\alpha^2+1)/\gamma_r$. By substituting the three correlation functions (11a)–(11c) into (12) and expanding to first order we thus find (for $t > 0$)

$$\begin{aligned} G_E(t) &= \left\{1-\frac{D(\alpha^2+1)}{4\gamma_r}\right\}e^{-(1/2)D(\alpha^2+1)t} \\ &\quad + D\left\{\frac{\alpha^2+1}{4\gamma_r}\right\}e^{-\gamma_{\text{eff}}t}\cos(\omega_r t) \\ &\quad + D\left\{\frac{3\alpha^2-1-4i\alpha(\gamma_n/\gamma_r)}{4\omega_r}\right\}e^{-\gamma_{\text{eff}}t}\sin(\omega_r t) \end{aligned} \quad (13)$$

where we have introduced the effective damping rate [6]

$$\gamma_{\text{eff}} = \gamma_r + \left\{\frac{D(\alpha^2+1)}{2}\right\}. \quad (14)$$

A Fourier transformation of this expression directly yields the optical spectrum of the (single-mode) laser. The first term in (13) describes the (long-term) diffusion of the optical phase and leads to a fundamental lower limit for the width of the central laser line [4]. The other terms in (13) oscillate in time as $\cos(\omega_r t)$ and $\sin(\omega_r t)$ and result in the formation of sidebands around the central laser line. Only the phase fluctuations contribute to the fundamental linewidth. They also dominate the relaxation oscillation sidebands if we assume, as usual, that $\alpha^2 >> 1$. In fact the relative importance of the correlation functions listed in (11) follows the hierarchy α^2, α, 1. This explains why often only the phase fluctuations are taken into account [6], an approach that intrinsically leads to a symmetric spectrum.

When (13) is Fourier transformed the following expression for the spectrum is found, if again terms smaller by a factor $(\gamma_r/\omega_0)^2$ are discarded,

$$\begin{aligned} G_E(\omega) &= \frac{D(\alpha^2+1)}{\omega^2+\left[\frac{D(\alpha^2+1)}{2}\right]^2}\left(1-\frac{D(\alpha^2+1)}{4\gamma_r}\right) \\ &\quad + \frac{D(\alpha^2+1)/4}{(\omega-\omega_0)^2+\gamma_{\text{eff}}^2}\left\{1-\frac{4\alpha}{\alpha^2+1}\left(\frac{\gamma_n}{\omega_0}\right) - \left(\frac{2\alpha^2-2}{\alpha^2+1}\right)\left(\frac{\omega-\omega_0}{\omega_0}\right)\right\} \\ &\quad + \frac{D(\alpha^2+1)/4}{(\omega+\omega_0)^2+\gamma_{\text{eff}}^2}\left\{1+\frac{4\alpha}{\alpha^2+1}\left(\frac{\gamma_n}{\omega_0}\right) + \left(\frac{2\alpha^2-2}{\alpha^2+1}\right)\left(\frac{\omega+\omega_0}{\omega_0}\right)\right\}. \end{aligned} \quad (15)$$

In the considered limit the factor $(1 - D(\alpha^2 + 1)/4\gamma_r)$ in (15) is almost unity. Notice that $G_E(\omega)$ is the shifted optical spectrum, i.e., the actual spectrum is found by substituting $\omega \rightarrow \omega - \omega_l$. The above equation for the optical spectrum is new and is the most important theoretical result from this paper. It is valid under the quite general assumption that $D(\alpha^2 + 1) << \gamma_r << \omega_r$. From this equation the following conclusions can be drawn

1) The spectrum consists of two broad bands centered around a (narrow) central line at a frequency distance $\Delta\nu \approx \omega_0/(2\pi)$. The width of the central line reflects the effect of phase diffusion and is often called the (modified) Schawlow–Townes linewidth of the laser. Its full width at half maximum (FWHM) is given by $D(\alpha^2 + 1)/(2\pi)$, which is via D inversely proportional to the optical output power of the laser [4]. The FWHM of the sidebands is $1/\pi$ times the effective damping rate γ_{eff}. It thus reflects the damping of the relaxation oscillations, but is additionally broadened by phase diffusion.

2) The relative intensity of the sidebands with respect to the central laserline is (for $\alpha >> 1$) given by

$$\frac{G_E(\omega = \omega_0)}{G_E(\omega = 0)} \approx \left\{\frac{D(\alpha^2 + 1)}{4\gamma_{\text{eff}}}\right\}^2 \tag{16}$$

which is the square of half the ratio of the width of the central laser line and that of the sidebands. Thus the spectral intensity and the width of the sidebands are not independent parameters, but are directly related: the stronger the damping, the weaker the sidebands [see (16)].

3) The Lorentzian wing of the central line still has an intensity $D(\alpha^2 + 1)/\omega_0^2$ at the sidebands, which occur at $\Delta\nu \approx \pm\omega_0/(2\pi)$, while the superimposed maxima are roughly $D\alpha^2/4\gamma_{\text{eff}}^2$. The original assumption $\gamma_r << \omega_0$ corresponds with the situation that the Lorentzian wing of the central laserline is much weaker than the sideband maxima. Equation (15) also shows that the sidebands do not have a perfect Lorentzian shape. They contain a weak asymmetric part that leads to a shift of the maxima and to additional "filling" of the spectrum between the sidebands and the central laserline.

4) The coupling between the amplitude and phase-fluctuations of the electric field, as was expressed in the function $\langle[u(t' + t) + u(t')][\phi(t' + t) - \phi(t')]\rangle$ and described by the α parameter, leads to an asymmetry between the sidebands. When the sidebands are well resolved the amount of asymmetry can be found by using (15). For the ratio of the spectral intensity of both sidebands we find

$$\frac{G_E(\omega = -\omega_0)}{G_E(\omega = \omega_0)} \approx 1 + \left\{\frac{8\alpha}{\alpha^2 + 1}\right\}\left\{\frac{\gamma_n}{\omega_0}\right\}. \tag{17}$$

Since α is positive [11], the low-frequency sideband is stronger than the high-frequency one. The measured spectral asymmetry can thus be used to determine the α parameter of a semiconductor laser. In the limiting cases where α is zero or very large, the spectrum will be symmetric. The spectral asymmetry will be relatively large if the relaxation oscillations are heavily damped; in that case, however, the sidebands will also be relatively weak. The appearance of γ_n instead of γ_r in (17) shows that even when D, α, γ_r, and ω_r are kept the same, and the width of the central laser line as well as the symmetric part of the relaxation oscillation sidebands remain unchanged, the spectral asymmetry is affected by nonlinear gain. The spectral asymmetry is reduced when damping due to nonlinear gain becomes relatively more important [see (10) and (17)].

IV. Heterodyne Detection

We have used heterodyne detection to accurately measure the spectrum of light from a Hitachi HLP1400 (CSP-type) AlGaAs laser, operating around 830 nm. The experimental setup is sketched as Fig. 1. With a beamsplitter light from the laser under study is mixed with light from a narrow-band tunable reference laser, acting as local oscillator. Optical isolators are placed in both beams to prevent feedback. After spatial filtering with a short piece of single-mode fiber the combined intensity of the two beams is measured with a low-noise photodiode. The photodiode signal is routed through a bandpass filter ($Q = 5$) centered around 50 kHz, after which the root-mean-square (rms) amplitude of the filtered signal is detected with an ac voltmeter. Filter and ac voltmeter are combined in a lock-in amplifier. Part of the light from the reference laser is directed through a Fabry–Perot etalon with a free-spectral range of 250 MHz thus providing reference markers to calibrate the frequency scan.

The total intensity detected by the photodiode, being proportional to the square of the sum of the optical fields, contains a term oscillating at the frequency difference between both lasers. By observing the rms amplitude of the filtered photodiode signal as a function of the frequency of the scanning reference laser one probes the spectral amplitude of the laser under investigation.

As a reference laser we use a home-built external cavity diode laser based on a standard design of a single-sided antireflection-coated solitary laser and a grating for frequency tuning [20]. With the grating, which can be rotated manually or by means of a piezoelement, our laser is tunable from 820 to 868 nm. Fine tuning of the cavity length is done with a glass plate, mounted on a galvo scanner. Suitably combining the rotation of the glass plate with that of the grating leads to a linear scan of the laser frequency over typically 15 GHz in a few seconds. Via self-heterodyne detection [21] we have measured the linewidth of the external cavity laser to be typically 50 kHz.

One should realize that the spectrum determined with heterodyne detection differs from spectra taken with, e.g., a spectrometer or a Fabry–Perot etalon in the sense that the spectral amplitude $|E(\omega)|$ is measured, instead of the spectral intensity $|E(\omega)|^2$. This partially explains the extreme sensitivity of heterodyne detection. For easy comparison of our data with other experiments we will systematically plot the square of the measured rms amplitude.

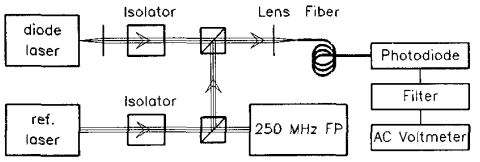

Fig. 1. Experimental setup used for heterodyne detection of the spectrum.

V. Experimental Results

A typical result of a heterodyne experiment is shown as Fig. 2, where the square of the rms amplitude of the filtered photodiode signal is plotted versus the frequency difference between the reference laser and the Hitachi laser under study. The latter was operating 6.5 mA above its 53.5 mA threshold and produced 1.6 mW output power per facet. The central peak is fitted by a Lorentzian curve with a HWHM of 34 MHz as shown in Fig. 2(a). The fit is excellent in the wings, but seems a bit narrow around the top.

Additional features are visible in Fig. 2(b), which shows the same spectrum with different horizontal and vertical scales. The vertical scale has been expanded by more than a factor 100 as compared to Fig. 2(a). The sharp features near ± 1.4 and ± 2.8 GHz are "ghosts" from the central laser line, which appear because the external cavity laser, used as local oscillator, is not truly operating single mode, having a small fraction of its intensity in other longitudinal modes. The 1.41 GHz mode spacing of the external-cavity laser can be nicely observed. The strengths of these ghosts changes with the alignment of the external-cavity laser. Interesting physics is contained in the broad sidebands near ± 1.9 GHz, denoting the presence of relaxation oscillations. The quality of this measurement, which took less then one minute, is evident: although the spectral intensity of the sidebands is less than 1% of that of the central peak, the sidebands are well resolved and even features with a spectral intensity as low as 10^{-4} of that of central line are observable.

The data points are excellently fit by the theory presented earlier if we use the following parameters: $D(\alpha^2 + 1)/(2\pi) = 68$ MHz, $\nu_0 = 1.94$ GHz, and $\gamma_{\text{eff}}/(2\pi) = 225$ MHz. The fitting procedure worked as follows. First, the combination $D(\alpha^2 + 1)/(2\pi)$, which can be recognized as the FWHM laser linewidth, was adjusted to fit the strong central laser line. Then, the frequency and effective damping rate of the relaxation oscillations ν_0 and γ_{eff} were adjusted to fit the symmetric part of the relaxation oscillation sidebands. Both parameters could be deduced from the fit with an accuracy better than 5%. We stress that the height and width of the observed sidebands can not be independently fitted, but are intimately linked in the theory presented above. Our measurement is thus an accurate check of that theory.

The two other parameters that appear in (15) are γ_n and α separately. The values of these parameters is mainly reflected in the spectral asymmetry between the low- and high-frequency sideband. If the nonlinear gain would be weak, γ_n could be set equal to γ_r and the measured asymmetry could be directly used to determine α. For the experiment displayed in Fig. 2 we measure the spectral intensity of the low-frequency sideband to be $18 \pm 3\%$ larger than that of the high-frequency sideband. The fit shown in Fig. 2(b) has been obtained using $\gamma_n = \gamma_r$ and $\alpha = 5.0$ [see also (17)].

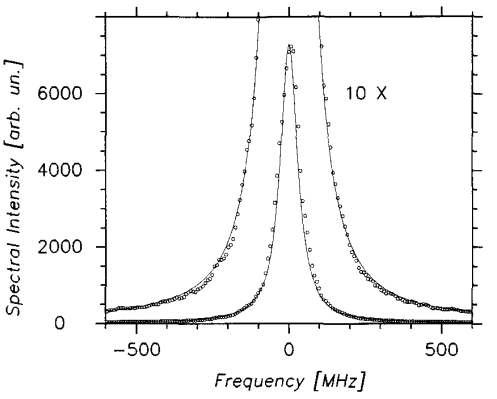

(a)

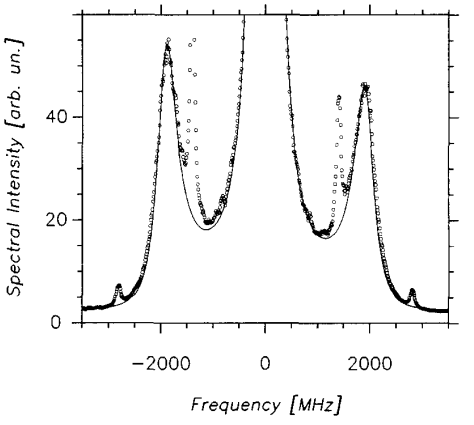

(b)

Fig. 2. Typical spectrum of a Hitachi HLP1400 (CSP) AlGaAs laser operating at a total output power of 3.2 mW. Plotted is the spectral intensity, i.e., the square of the signal measured by the ac voltmeter in Fig. 1 versus the frequency of the reference laser. In (a) the central line is fitted to a Lorentzian curve with a HWHM of 34 MHz. (b) is a different representation of the same data showing the sidebands resulting from relaxation oscillations.

The effect of α on the spectral shape is demonstrated in Fig. 3, where theoretical spectra have been calculated for $\alpha = 0$, 5, and 10, respectively. From this plot the contribution of the non-Lorentzian part to the sidebands {see (15)} is evident: for $\alpha = 5$ and 10 the non-Lorentzian components lead to an increase of the spectral intensity between the sidebands and the central line, in addition to the underlying Lorentzian wings of the central line, and to a reduction of the spectral intensity outside the sidebands. Unfortunately neither the spectral asymmetry of the sidebands nor their individual shapes depend critically on α for large values of this parameter. The difference

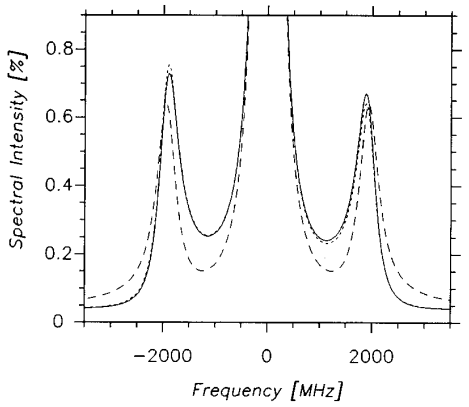

Fig. 3. The effect of the α-parameter on the relaxation oscillation sidebands is calculated for $D(\alpha^2 + 1)/(2\pi) = 68$ MHz, $\nu_0 = 1.94$ GHz, $\gamma_{cll}/(2\pi) = 225$ MHz, $\gamma_n = \gamma_r$ and for $\alpha = 0$ (long-dashed), $\alpha = 5$ (short-dashed), and $\alpha = 10$ (solid).

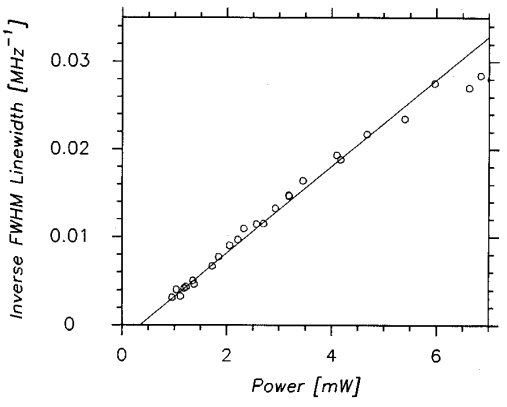

Fig. 4. The inverse of the measured linewidth plotted as a function of the total output from both facets.

between the short-dashed curve ($\alpha = 5$) and the solid curve ($\alpha = 10$) is not at all drastic: only a small reduction in asymmetry is observable. Therefore, a very precise measurement of the asymmetry of the sidebands is necessary to determine the α parameter of a semiconductor laser. Furthermore the equation that describes the spectral asymmetry [(17)] actually contains a factor γ_n instead of γ_r and, whereas γ_r can be relatively easily determined from the width and relative strength of the relaxation oscillation sidebands, γ_n is more difficult to determine. In the next section we will discuss how this quantity can be estimated from a study of the power dependence of both ν_0 and γ_r [see Figs. 6 and 7]. Based on that analysis we estimate that at 3.2 mW output power the ratio $\gamma_n/\gamma_r \approx 0.6$. When this value, together with the measured $18 \pm 3\%$ asymmetry, is inserted into (17) one finds $\alpha = 3 \pm 1$. Measurements at different output power gave similar results.

Accurate measurement of the spectral asymmetry of the relaxation oscillation sidebands is a new technique to determine the α parameter of a semiconductor laser. Several other techniques have been reviewed by Osinski and Buus [23]. Our value falls well within the spread of values cited in [23]. Compared to techniques based on FM–AM modulation [24] or providing feedback [25] our method has the advantage that the measurements are performed on an *unperturbed* laser [26]. In this case spontaneous emission is the only, internal driving force that keeps pushing the laser out of its equilibrium. Clearly the technique will work for any semiconductor laser with reasonably pronounced relaxation oscillations. The technique is most sensitive for lasers with a small α.

We have measured the spectrum of our Hitachi laser by heterodyne detection for many other currents than that used in Fig. 2. In Fig. 4 the inverse of the measured FWHM width of the central line $\Delta\nu$ is plotted versus the total output power of the laser. The measurements are fitted by a straight line as theory predicts the linewidth of a single-mode laser to be inversely proportional to the output power. We interpret the 0.4 ± 0.1 mW crossing with the x axis as the (spontaneous emission) power present in the other nonlasing longitudinal modes. The slope of the straight line in Fig. 4 can be used to obtain an additional rough estimate of the α parameter, since $\Delta\nu = D(\alpha^2 + 1)/(2\pi)$. Combining the measured "linewidth-power product" of 204 ± 12 MHz · mW with a reasonable guess of the laser parameters appearing in (9), for which we use $n_{sp} = 1.5$, $\Gamma_c = 8.6 \times 10^{11}$ s^{-1}, and $K = 1.13$, we find $\alpha = 5 \pm 1$ [22]. The average number of photons in the laser mode, appearing in (9), was calculated from the output power, using (19) listed below. The large uncertainty in some of these parameters make this estimate of α less reliable than the value extracted from the asymmetry of the relaxation oscillation sidebands. For our laser both estimates are consistent.

A close study of the position and shape of the spectral sidebands of our Hitachi laser as a function of the output power yields a wealth of information on the dynamics of the relaxation oscillations. When the output power increases the central line narrows down and the sidebands recede from the central line and become less pronounced. The spectra plotted in Fig. 5 illustrates this trend. The solid curves are fits through the measured points. The total output power from both facets is marked in the upper right-hand corner for each spectrum. At 2.7 mW total output power the spectral intensity in the sidebands is about one percent of that in the central line. This relative strength grows quickly when the output power is reduced, while the sidebands move towards a central line of increasing width. The theory gives a reasonable fit down to 1.5 mW. At the lowest powers the theory presented above, which was based on a first-order expansion in $D(\alpha^2 + 1)/\gamma_r$, is no longer valid. The sidebands seem to merge with the central line when they become overdamped. The combined line can then be well fitted with a simple Lorentzian line as is demonstrated in Fig. 5(d).

In Fig. 6 the square of the measured relaxation oscillation frequency ν_0 is plotted versus the total output power

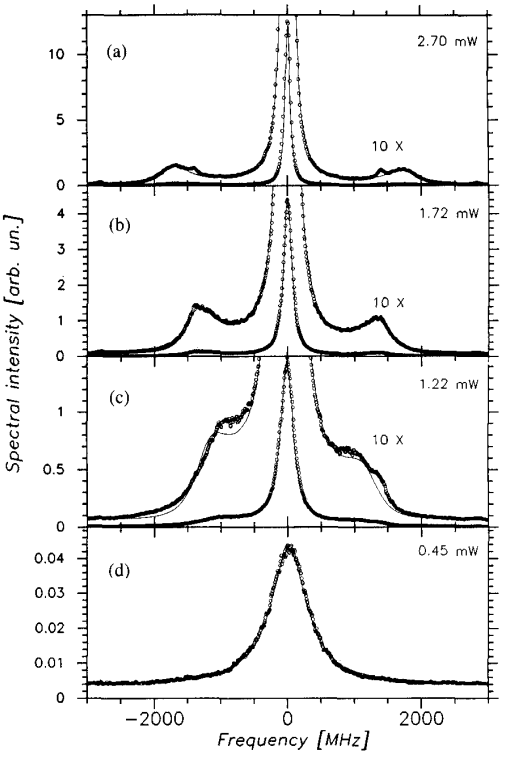

Fig. 5. Spectra of a Hitachi HLP1400 laser taken at decreasing output powers. The upper three spectra are fitted with the linearized theory discussed in this article. The lower spectrum (d) is fitted by a simple Lorentzian line.

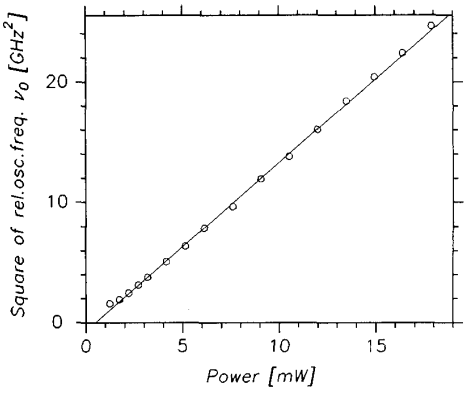

Fig. 6. The square of the measured relaxation oscillation frequency plotted versus the total output power of the laser. The linear behavior represents the prediction by theory. The crossing with the x axis at 0.5 mW is due to the power present in the other (nonlasing) longitudinal modes.

from both facets. The linear dependence predicted by (10.b) fits the data well. The 0.5 mW crossing with the x axis reflects the (spontaneous emission) power present in the other nonlasing longitudinal modes. This value is comparable to the crossing which we found when plotting the inverse of the measured width of the central line versus the total output power (Fig. 4).

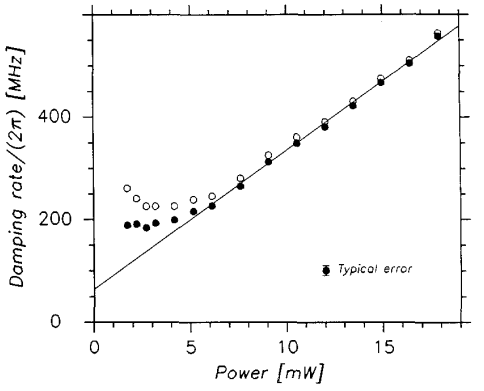

Fig. 7. The measured damping of the relaxation oscillation sidebands plotted versus the total output power of the laser. The open circles denote the effective damping rate, while the filled circles are corrected for the width of the central line. The linear fit gives the spontaneous lifetime τ_{sp} as well as the additional damping resulting from the differential gain and the gain saturation.

In Fig. 7 the open circles denote the fitted effective damping $\gamma_{\text{eff}}/(2\pi)$, which is plotted versus the total output power. By subtracting the HWHM of the central line one finds the actual damping $\gamma_r/(2\pi)$ of the relaxation oscillations [see (14)] indicated by filled circles. The experimental accuracy of the data points is typically 5%, as denoted by the error bar, degrading to 10% for the lowest power. Theory predicts a linear dependence of the damping rate on the output power as indicated by the drawn straight line [see (10c)]. At low powers (<4 mW) the measurements deviate from the theoretical model, but this could be expected on account of two reasons. First, the assumption that the laser line is narrow as compared to the width of the sidebands does not hold at the lowest powers. Second, laser operation becomes multimode close to threshold. At 1.5 mW total output power the intensity of the second-strongest mode is already 10% of that of the main mode and this ratio increases strongly below 1.5 mW. Also notice that for all plotted points the frequency ν_0 is at least a factor of 5 larger than the damping $\gamma_r/(2\pi)$ thus validating the assumption $(\gamma_r/\omega_0)^2 \ll 1$.

Notice that the deviation of the theoretically calculated damping rate and the experimentally measured value already occurs at an output power below 4 mW, whereas the quality of the calculated fit still matches very well at this output power (see Figs. 2 and 5). Apparently the deviations from the theoretical model first occur in the value of the fitted relaxation oscillation damping rate; only at very low power deviations in the *shape* of the spectrum are observable [see Fig. 5(c)].

Combination of the power dependence of the relaxation oscillation frequency and damping rate as presented in Figs. 6 and 7 allowed us to separately determine the spontaneous lifetime τ_{sp} and the dependence of the gain on both carrier density (ξ) and optical intensity (κ_S). The spontaneous lifetime is related to the intensity-independent contribution to the damping rate, which is found by extrapolating the linear dependence of the damping rate

versus the total output power, which fits nicely above 4 mW, to 0.4 mW, being the power in the nonlasing longitudinal modes. The obtained power-independent damping of $\gamma_r/(2\pi) = 75 \pm 15$ MHz yields a spontaneous lifetime $\tau_{sp} = 1.1 \pm 0.3$ ns.

From the slopes of Figs. 6 and 7 the increase in relaxation oscillation frequency and damping as a function of output power is found to be $d\nu_0^2/dP_{out} = 1.39$ $(\text{GHz})^2/\text{mW}$ and $d(\gamma_r/2\pi)/dP_{out} = 27$ MHz/mW, respectively. These values are obtained directly from the data and are limited only by experimental error. Combination of these two values allows one to quantitatively determine the differential gain ξ as well as the gain saturation coefficient κ_S. Using (10b) and (10c) one finds

$$\frac{d\nu_0^2}{dS_0} = \left(\frac{\Gamma_c}{4\pi^2\Gamma}\right)\xi \tag{18a}$$

$$\frac{d(\gamma_r/2\pi)}{dS_0} = \frac{1}{4\pi}\left(\frac{\xi}{\Gamma} + \Gamma_c\kappa_S\right). \tag{18b}$$

In order to compare the slopes of the straight lines in Figs. 6 and 7 with the above equations we express the total output power of the laser in the photon density S_0, using the relation

$$\frac{dP_{out}}{dS_0} = \eta_{ext} h\nu \Gamma_c V/\Gamma. \tag{19}$$

Here η_{ext} is the outcoupling efficiency, being the fraction of generated photons emitted by the laser, the rest being dissipated through internal losses. Unfortunately this relation contains several laser parameters, like the active volume V and the confinement factor Γ, that are only roughly known for our Hitachi HLP1400 laser. We could determine the outcoupling efficiency $\eta_{ext} = 0.35$ from the relation between output power and current, assuming the internal efficiency, i.e., the conversion of electrons into photons, to be close to unity. The cavity loss rate $\Gamma_c = 8.6 \times 10^{11}\ \text{s}^{-1}$ is found from gain spectra below threshold [22]. These values could be determined with better accuracy ($\pm 5\%$) than the parameters V and Γ that also appear in (19). Thus we have decided to first substitute the values of η_{ext} and Γ_c into the equations and postpone substitution of V and Γ. This yields

$$\frac{\xi}{V} = 0.45 \times 10^4\ \text{s}^{-1} \tag{20a}$$

$$\frac{\xi}{V} + \frac{\Gamma\Gamma_c\kappa_S}{V} = 2.44 \times 10^4\ \text{s}^{-1}. \tag{20b}$$

Comparing these values we conclude that the differential gain contributes only about 20% of the increase in damping rate towards higher powers, the rest being due to gain saturation. In our AlGaAs laser gain saturation apparently dominates the damping at high output powers.

Finally, we insert the two laser parameters we know least accurate, V and Γ. Studies using the Hitachi HLP1400 have been reported by many authors, but the specified dimensions of the active volume amazingly differ from paper to paper [1], [4], [27], [28]. For this reason we decided to measure the optical mode volume; in fact, the optical mode volume V/Γ is more important for the dynamics of the relaxation oscillations than the active volume V. The optical near field is intimately linked with the far field, which has the familiar elliptical Gaussian profile with (HWHM) opening angles of 0.25 rad perpendicular and 0.10 rad parallel to the active layer. For the optical field inside the laser we thus find an effective cross section (based on a rectangular intensity profile) of 0.78 μm $\times$ 2.1 μm. The length of the laser is measured to be 309 μm. From the so obtained optical mode volume $V/\Gamma = 5.1 \times 10^{-10}$ cm^3 we find that at 1 mW total output power the photon density is approximately $S_0 = 2.7 \times 10^{13}$ cm^{-3} [see (19)]. Knowledge of the confinement factor or the related thickness of the active layer is needed to calculate V from V/Γ and determine ξ from (20a). The bulk differential gain ξ/Γ is, however, simply found by multiplying both sides of (20a) by the optical mode volume V/Γ. We thus find $\xi/\Gamma = 2.3 \times 10^{-6}$ cm^3/s, which is comparable to both the value of 2.2×10^{-6} cm^3/s mentioned by Petermann [29] and the value of 2.5×10^{-6} mentioned by Vahala *et al.* [1]. Combining (20b) with the above data we estimate the saturation gain coefficient to be $\kappa_S = 1.2 \times 10^{-17}$ cm^3. For our laser this corresponds to a saturation coefficient (referring to the total output power) of $\kappa_P = 0.32\ \text{W}^{-1}$. Our values are smaller than the value of $0.65\ \text{W}^{-1}$ mentioned in [30], but comparable to the value $\kappa_S = 1.7 \times 10^{-17}$ cm^3 mentioned in [31] and almost a factor 2 larger than the value $\kappa_S = 0.7 \times 10^{-17}$ cm^3 mentioned in [32]. The spread in these values is possibly due to the fact that gain saturation is not a pure bulk parameter, but depends also on the device architecture [32].

VI. Conclusion

Starting from the linearized laser equations, an expression was obtained for the spectral lineshape of a single-mode semiconductor laser, which consists of a central line and two sidebands resulting from relaxation oscillations. The theoretical expressions provide an accurate fit for spectra of a Hitachi HLP1400 AlGaAs laser measured with optical heterodyne detection. From the asymmetry in the sidebands we were able to derive the α parameter of the laser. The relative contribution of nonlinear gain to the relaxation-oscillation damping has to be known to perform this calculation. We find $\alpha = 3 \pm 1$.

The spectra yield a wealth of information on the dynamics of the relaxation oscillations. A study of the relaxation oscillation frequency versus output power yielded a bulk differential gain of $\xi/\Gamma = 2.3 \times 10^{-6}$ cm^3/s. The damping rate was seen to increase almost linearly with the output power. From this relation we could extract the spontaneous lifetime $\tau_{sp} = 1.1 \pm 0.3$ ns as well as the gain saturation coefficient $\kappa_S = 1.2 \times 10^{-17}$ cm^3 or $\kappa_P = 0.32\ \text{W}^{-1}$. We found that at high output powers gain sat-

uration dominates the damping of the relaxation oscillations.

ACKNOWLEDGMENT

We thank D. Bouwmeester for his measurement of the far-field profile.

REFERENCES

[1] K. Vahala, C. Harder, and A. Yariv, "Observation of relaxation resonance effects in the field spectrum of semiconductor laser," *Appl. Phys. Lett.*, vol. 42, pp. 211-213, 1983.

[2] K. Vahala and A. Yariv, "Semiclassical theory of noise in semiconductor lasers—Part I and II," *IEEE J. Quantum Electron.*, vol. QE-19, pp. 1096-1109, 1983.

[3] B. Daino, P. Spano, M. Tamburrini, and S. Piazzolla, "Phase noise and spectral line shape in semiconductor lasers," *IEEE J. Quantum Electron.*, vol. QE-19, pp. 266-270, 1983.

[4] C. H. Henry, "Theory of the phase noise and power spectrum of a single-mode injection laser," *IEEE J. Quantum Electron.*, vol. QE-19, pp. 1391-1397, 1983.

[5] Y. Yamamoto, "AM and FM quantum noise in semiconductor lasers—Part I and II," *IEEE J. Quantum Electron.*, vol. QE-19, pp. 34-58, 1983.

[6] S. Piazzolla and P. Spano, "Analytical evaluation of the line shape of single-mode semiconductor lasers," *Opt. Commun.*, vol. 51, pp. 278-280, 1984.

[7] K. Petermann, *Laser diode modulation and noise*. Dordrecht: Kluwer Academic, 1988.

[8] R. J. Lang, H. P. Mayer, H. Schweizer, A. P. Mozer, P. Panknin, and W. Elsässer, "Measurement of relaxation oscillation resonance, damping, and nonlinear gain coefficient from the sidebands in the field spectrum of a 1.3 μm InGaAsP distributed feedback laser," *Appl. Phys. Lett.*, vol. 54, pp. 1845-1847, 1989.

[9] R. Lang and K. Kobayashi, "External optical feedback effects on semiconductor injection laser properties," *IEEE J. Quantum Electron.*, vol. QE-16, pp. 347-355, 1980.

[10] K. Kikuchi, "Lineshape measurement of semiconductor lasers below threshold," *IEEE J. Quantum Electron.*, vol. 24, pp. 1814-1817, 1988.

[11] $\alpha = (\partial G_i/\partial N)/(\partial G_r/\partial N) = -(\partial \chi_r/\partial N)/(\partial \chi_i/\partial N)$, where χ_r and χ_i are, respectively, the real and imaginary part of the susceptibility. With our definitions α is positive for a semiconductor laser.

[12] A. P. Bogatov, P. G. Eliseev, and B. N. Sverdlov, "Anomalous interaction of spectral mosed in a semiconductor laser," *IEEE J. Quantum Electron*, vol. QE-11, pp. 510-515, 1975.

[13] C. B. Su, "Nonlinear gain caused by cavity standing wave dielectric grating as an explanation of the relationship between resonance frequency and damping rate of semiconductor diode lasers," *Appl. Phys. Lett.*, vol. 53, pp. 950-952, 1988.

[14] M. P. Kesler and E. P. Ippen, "Subpicosecond spectral gain dynamics in AlGaAs laser diodes," *Electron. Lett.*, vol. 24, pp. 1102-1103, 1988.

[15] R. Frankenberger and R. Schimpe, "Measurement of the gain saturation spectrum in InGaAsP diode lasers," *Appl. Phys. Lett.*, vol. 57, pp. 2520-2522, 1990.

[16] G. P. Agrawal, "Intensity dependence of the linewidth enhancement factor and its implications for semiconductor lasers," *IEEE Photon. Technol. Lett.*, vol. 1, pp. 1391-1397, 1983.

[17] J. S. Cohen and D. Lenstra, "Spectral properties of the coherence collapsed state of a semiconductor laser with delayed optical feedback," *IEEE J. Quantum Electron.*, vol. 25, pp. 1143-1151, 1989.

[18] G. P. Agrawal and N. K. Dutta, *Long-wavelength semiconductor lasers*. New York: Van Nostrand Reinhold, 1986.

[19] W. A. Hamel and J. P. Woerdman, "Observation of enhanced fundamental linewidth of a laser due to nonorthogonality of its longitudinal eigenmodes," *Phys. Rev. Lett.*, vol. 64, pp. 1506-1509, 1990.

[20] F. Favre and D. LeGuen, "82 nm of continuous tunability for an external cavity semiconductor laser," *Electron. Lett.*, vol. 27, pp. 183-184, 1990.

[21] L. E. Richter, H. I. Mandelberg, M. S. Kruger, and P. A. McGrath, "Linewidth determination from self-heterodyne measurements with subcoherence delay times," *IEEE J. Quantum Electron.*, vol. QE-22, pp. 2070-2074, 1986.

[22] W. A. Hamel, M. Babeliowsky, and J. P. Woerdman, "Diagnostics of asymmetrically coated semiconductor lasers," *IEEE Photon. Technol. Lett.*, vol. 3, pp. 600-602, 1991.

[23] M. Osinski and J. Buus, "Linewidth broadening factor in semiconductor lasers—An overview," *IEEE J. Quantum Electron.*, vol. QE-23, pp. 9-29, 1987.

[24] C. Harder, K. Vahala, and A. Yariv, "Measurement of linewidth enhancement factor α of semiconductor lasers," *Appl. Phys. Lett.*, vol. 42, pp. 328-330, 1983.

[25] C. H. Shin, M. Teshima, and M. Ohtsu, "Novel measurement method of linewidth enhancement factor in semiconductor lasers by optical self-locking," *Electron. Lett.*, vol. 25, pp. 28-29, 1989.

[26] K. Kikushi and T. Okoshi, "Estimation of linewidth enhancement factor of AlGaAs lasers by correlation measurement between FM and AM noises," *IEEE J. Quantum Electron.* vol. QE-21, pp. 669-673, 1985.

[27] M. Serenyi, E. O. Göbel, and J. Kuhl, "Inhomogeneous gain saturation in a mode-locked semiconductor laser," *Appl. Phys. Lett.*, vol. 53, pp. 169-171, 1988.

[28] The Hitachi company specifies the dimensions of the active layer to be roughly 0.05 μm $\times$ 6 μm $\times$ 300 μm. The confinement factor they specify is $\Gamma = 0.13$.

[29] $\xi/\Gamma = 2.2 \times 10^{-6}$ cm^3/s is determined from the ratio a/v_g mentioned on p. 21 of [7].

[30] B. C. Johnson and A. Mooradian, "Observation of gain compression in a GaAlAs diode laser through a picosecond transmission measurement," *Appl. Phys. Lett.*, vol. 49, pp. 1135-1137, 1986. The value $\kappa_P = 1.3\ \mathrm{W}^{-1}$ mentioned in this paper refers to the single-sided output power. When referring to the total output power it corresponds to $\kappa_P = 0.65\ \mathrm{W}^{-1}$.

[31] A. P. DeFonzo and B. Gomatam, "Gain nonlinearities in semiconductor lasers and amplifiers," *Appl. Phys. Lett.*, vol. 56, pp. 611-613, 1989.

[32] R. S. Tucker and D. J. Pope, "Circuit modeling of the effect of diffusion on damping in a narrow-stripe semiconductor laser," *IEEE J. Quantum Electron.*, vol. QE-19, pp. 1179-1183, 1983.

M. P. van Exter, for a photograph and biography, see this issue, p. 1469.

W. A. Hamel, for a photograph and biography, see this issue, p. 1469.

J. P. Woerdman, for a photograph and biography, see this issue, p. 1469.

B. R. P. Zeijlmans, photograph and biography not available at the time of publication.